Sachdev-Ye-Kitaev Model in a Quantum Glassy Landscape

Surajit Bera[1], Jorge Kurchan[2], and Marco Schirò[1]
[1] *JEIP, UAR 3573 CNRS, Collège de France, PSL Research University, 11 Place Marcelin Berthelot, 75321 Paris Cedex 05, France*
[2] *Laboratoire de Physique de l'École Normale Supérieure, ENS, Université PSL, CNRS, Sorbonne Université, Université de Paris, F-75005 Paris, France*
(Dated: September 30, 2025)

We study a generalization of 'Yukawa models' in which Majorana fermions, interacting via all-to-all random couplings as in the Sachdev-Ye-Kitaev (SYK) model, are parametrically coupled to disordered bosonic degrees of freedom described by a quantum $p-$spin model. The latter has its own non-trivial dynamics leading to quantum paramagnetic (or liquid) and glassy phases. At low temperatures this setup results in SYK behavior within each metastable state of a rugged bosonic free energy landscape, the effective fermionic couplings being different for each metastable state. We show that the boson-fermion coupling enhances the stability of the quantum spin-glass phase and strongly modifies the imaginary-time Green's functions of both sets of degrees of freedom. In particular, in the quantum spin glass phase, the imaginary-time dynamics is turned from a fast exponential decay characteristic of a gapped phase into a much slower dynamics. In the quantum paramagnetic phase, on the other hand, the fermions imaginary-time dynamics get strongly modified and the critical SYK behavior is washed away.

I. INTRODUCTION

In recent years, the Sachdev-Ye-Kitaev (SYK) model has attracted significant attention in a wide range of research fields [1–7]. The SYK model features random all-to-all interactions among q Majorana or complex fermions. SYK and its variants exhibit several remarkable features: they provide a solvable example of non-Fermi liquid behavior [8, 9], offer insight into the mechanism behind strange and Planckian metallicity [10–14], saturate the bound on quantum chaos [4, 15, 16], and capture essential aspects of black hole dynamics through holographic correspondence [17, 18]. Its solvability in the large-N limit, where N denotes the number of fermionic flavors, thus provides a powerful framework for exploring these diverse physical phenomena, in fields ranging from strongly correlated electron systems in condensed matter to holographic dualities in quantum gravity.

The SYK model originates as an effective theory from a spin-glass model, the quantum random Heisenberg model [19–21]. It can also be viewed as a fermionic analogue of another paradigmatic and exactly solvable mean-field spin-glass model—the quantum p-spin glass model [22–27]. This model involves random all-to-all couplings among p bosonic degrees of freedom, shares similar large-N saddle-point equations, and exhibits time-reparametrization symmetry [28–30], similar to the features of the SYK model. A key characteristic of such mean-field spin-glass systems is their rugged potential energy landscape, with the number of metastable minima or maxima scaling exponentially with system size N. The bosonic degrees of freedom can remain trapped in these metastable states for divergent times in the thermodynamic limit, effectively breaking ergodicity below a critical temperature and leading to spin-glass order.

The p-spin model has been extensively studied as a solvable glass [22, 31–33]. Its quantum model by itself exhibits a rich phase diagram [26] (see also [34, 35]). At low temperatures, the bosonic degrees of freedom condense into a spin-glass phase with broken ergodicity, characterized by one-step replica symmetry breaking (1-RSB) in the replica formalism framework. In contrast, at higher temperatures or under strong quantum fluctuations, the system enters a quantum paramagnetic phase with replica-diagonal order parameters. The phase diagram in the Γ–T plane has been studied in literature; we refer the reader to Ref. [26] for a detailed discussion, where Γ quantifies the strength of quantum fluctuations and T is the temperature of the bosonic system. The low-temperature metastable states are organized as in Fig 1: there are the very lowest in free energy that dominate the Gibbs-Boltzmann measure (and are described by a standard replica calculation), plus an exponentially increasing number with higher and higher free energies, up to a 'threshold' level where states are marginal, i.e. gapless: these states dominate the out of equilibrium dynamics after a quench [25, 36]. To avoid confusion, throughout this paper we shall use the word 'state a' to denote a distribution ρ_a that is stationary under dynamics and not decomposable into smaller stable ones (an object that could as well be classical), while one shall use 'eigenstate' to denote a quantum eigenstate of a Hamiltonian. The model has two types of paramagnetic solutions, namely a 'classical' paramagnet exits in high temperature or small Γ limit, and a 'quantum' paramagnet exists in low temperature at very high value of Γ.

In this work, we investigate how Majorana fermions with SYK-type all-to-all interactions evolve under the influence of background fluctuations arising from a disordered bosonic environment described by the quantum spherical p-spin glass model. To this end, we study a model of disordered fermion-boson interactions involving random all-to-all couplings. We consider a fermion-boson interaction term in which Majorana fermions interact via

SYK-type four-fermion interactions that are parametrically modulated by their coupling to bosonic degrees of freedom governed by a quantum spherical p-spin glass model. The quantum fluctuations of bosonic degrees of freedom directly influence the effective couplings among fermions. This setup captures the intuitive picture of SYK fermions evolving within the complex landscape of a mean-field spin-glass potential, effectively confined in different metastable valleys corresponding to local minima of the bosonic free energy (see Figure 1). At very low temperatures, the fermions become trapped in these minima and experience background fluctuations controlled by the spin-glass order.

We examine our model of disordered fermion-boson interactions, as described earlier, with the aim to address the following questions: How do fermions evolve across different regimes of the spin-glass phase diagram? How does fermionic feedback reshape the bosonic order parameters and correlations? Our focus and motivations differ from those in earlier studies of SYK coupled with bosonic fields. Prior work has studied Yukawa-type interactions[37], where fermions interact with critical bosonic fields associated with paramagnetic order parameters. Such models have been shown to give rise to a variety of strongly correlated phases, including superconductivity [38–40], non-Fermi liquid behavior with critical Fermi surfaces [41, 42], and quantum criticality [42, 43]. In parallel, supersymmetric extensions of the SYK model have also been investigated, where SYK fermions couple to their supersymmetric bosonic partners [6, 44–46]. In contrast, in our work we study the coupling of fermions to both non-critical (equilibrium glass) and critical (marginal glass[47]), glassy bosonic fields, revealing all to all coupled fermionic dynamics under fluctuating background, and uncovering novel feedback effects of fermion to spin-glass order.

The boson-fermion coupling has two main effects on the physics of our model. First, it modifies the phase diagram by enhancing the stability of the thermodynamic quantum spin-glass phase at finite quantum fluctuation Γ. Second, it strongly affects the imaginary-time correlation functions of both sets of degrees of freedom. In particular, in the quantum spin-glass phase the bosonic correlator at low-temperature is strongly renormalised and its exponential decay in imaginary-time washed out. In the quantum paramagnet phase on the other hand is the fermionic sector dynamics which is mostly affected and the SYK critical behavior is turned into a slow dynamics characterised by a flat correlation function.

The manuscript is organized as follows. In Sec. II, we introduce the coupled fermion-boson model, derive the large-N saddle-point equations, and briefly review key features of the decoupled spherical spin-glass and SYK models. In Sec. III, we present results for the spin-glass phase of the coupled system, followed by an analysis of the paramagnetic phase in Sec. IV. We conclude with a discussion in Sec. V. Additional technical details are provided in the Appendix.

II. MODEL

We consider the following Hamiltonian:

$$\mathcal{H} = \mathcal{H}_{\rm b}[s] + \mathcal{H}_{\rm int}[s,\chi], \tag{1}$$

where $\mathcal{H}_{\rm int}[s,\chi]$ denotes the interaction term between bosons (s) and Majorana fermions (χ). The bosonic part $\mathcal{H}_{\rm b}$ is given by the Hamiltonian of a quantum spherical p-spin glass model:

$$\mathcal{H}_{\rm b} = \sum_i \frac{\pi_i^2}{2M} + \sum_{i<j<k} J_{ijk} s_i s_j s_k. \tag{2}$$

Here, s_i and π_i are canonically conjugate variables satisfying the commutation relation $[s_i, \pi_j] = \mathrm{i}\hbar\delta_{ij}$, where $\hbar$ is the Plank constant. The coordinate s_i is continuous, taking values over the entire real line, $(-\infty, +\infty)$. In this work, we focus on the case $p = 3$, i.e., interactions involving three bosons. The all-to-all random couplings J_{ijk} are real variables drawn from a Gaussian distribution with zero mean and variance

$$\sigma_J^2 = \langle J_{ijk}^2 \rangle = \frac{J^2 \cdot 3!}{2N^2}.$$

To ensure the model remains non-trivial, we impose a spherical constraint:

$$\sum_i s_i^2 = N,$$

where N is the total number of bosonic modes. In the context of the p-spin glass model, the degrees of freedom s_i are often referred to as spin variables. Throughout this work, we use the terms "spin" and "boson" interchangeably to refer to the coordinate s_i.

The interaction between the bosonic coordinates s_i and the Majorana fermions χ_i is given by:

$$\mathcal{H}_{\rm int} = \sum_{i_1,\ldots,i_r} \sum_{mnpq} V_{i_1\ldots i_r}^{mnpq} \chi_m \chi_n \chi_p \chi_q \, s_{i_1} \ldots s_{i_r} \tag{3}$$

We do not expect the order $r > 0$ of the bosonic part to have a great impact, since the glassiness of bosons is given by the pure boson term. Here we concentrate on $r = 4$:

$$\mathcal{H}_{\rm int} = \sum_{ijkl} \sum_{mnpq} V_{ijkl}^{mnpq} \chi_m \chi_n \chi_p \chi_q \, s_i s_j s_k s_l. \tag{4}$$

The interaction tensor V_{ijkl}^{mnpq} is a real variable drawn from a Gaussian distribution with zero mean. It is symmetric under the exchange of any pair of bosonic indices (i, j, k, l) and antisymmetric under the exchange of any pair of fermionic indices (m, n, p, q). We assume that the number of bosonic and fermionic degrees of freedom is equal, i.e., both sets of indices range from 1 to N. The variance of V_{ijkl}^{mnpq} is given by:

$$\sigma_V^2 = \langle (V_{ijkl}^{mnpq})^2 \rangle = \frac{4! \cdot 3! \cdot V^2}{2N^7}. \tag{5}$$

This interaction term in Eq. (4), involving four Majorana fermions coupled to bosonic degrees of freedom, plays a crucial role in mimicking SYK-like fermionic dynamics in the presence of a fluctuating, glassy bosonic background. In particular, it leads, in the classical limit of the quantum spin-glass model, to an effective fermionic Hamiltonian of the form:

$$H_{\text{fermion}} \sim \mathcal{H}_{\text{SYK}} = \sum_{mnpq} \mathcal{J}_{mnpq} \chi_m \chi_n \chi_p \chi_q. \tag{6}$$

where the couplings $\mathcal{J}_{mnpq}$ are dynamically modulated by the fluctuating spin configuration $\vec{s}$ as:

$$\mathcal{J}_{mnpq} = \sum_{ijkl} V_{ijkl}^{mnpq} s_i s_j s_k s_l. \tag{7}$$

In the original SYK model, the couplings are drawn from a Gaussian distribution with zero mean and variance $\langle (\mathcal{J}_{mnpq})^2 \rangle = \mathcal{J}^2/2N^3$. To the extent that the s_i may be approximated as taking constant, static values, we are essentially back to the original SYK, with modified interactions. However, this must be interpreted with care in the quantum regime, since the bosonic variables $s_i(\tau)$ are quantum fields that fluctuate in imaginary time τ, even at zero temperature. In a later section, we will discuss how these quantum spin fluctuations modify the fermionic saddle-point equations compared to those of the original SYK model, and under what conditions the standard SYK saddle point for fermions can be recovered.

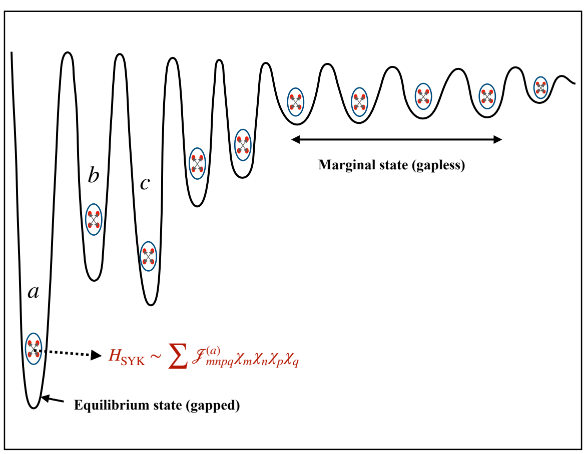

FIG. 1. **SYK Dots in the Energy Landscape of the Spin-Glass Model:** A schematic cartoon of the typical energy landscape of the p-spin-glass model is shown. The complex free-energy landscape consists of equilibrium states (gapped), an exponential number of metastable states, and marginal (threshold) states that are gapless. Each SYK dot is located in a different valley of this landscape, with a distinct fluctuating glassy background determined by the specific state $a, b, c, \ldots$. At very low T, the SYK dots are expected to occupy the low-lying minima (equilibrium states) in the semi-classical limit of the p-spin-glass model.

A. Large-N saddle point equations

The thermodynamics of the system described by the above Hamiltonian can be derived from the corresponding free energy functional. For disordered systems of this type, the free energy is self-averaging, meaning it becomes independent of a specific realization of disorder in the thermodynamic limit. Consequently, the disorder-averaged free energy at temperature T is given by:

$$F = -T\, \overline{\log Z}, \tag{8}$$

where the overline $(\overline{\cdots})$ denotes the average over different realizations of the disorder variables J_{ijk} and V_{ijkl}^{mnpq}.

To evaluate the disorder-averaged logarithm of the partition function, we employ the replica trick, write down the partion function for r copies (replicas) of the Hamiltonian Eq. 1 in path integral language, and then perform disorder average as described in detail in Appendix A. The effective partion function for r-replica reads as follows:

$$\overline{Z^r} = \int \mathcal{D}[G, \Sigma, Q, \Pi] e^{-S_{\text{eff}}[G,\Sigma,Q,\Pi]} \tag{9}$$

where the effective action is given by:

$$\begin{aligned} S_{\text{eff}} = & -N \operatorname{Tr}\ln\big(- G_{0,ab}^{-1} + \Sigma_{ab}\big) - \frac{N}{2} \operatorname{Tr}\ln\big(Q_{0,ab}^{-1} - \Pi_{ab}\big) \\ & + \frac{NV^2}{4} \int_{\tau,\tau'} \sum_{ab} G_{ab}^{\circ 4}(\tau,\tau') Q_{ab}^{\circ 4}(\tau,\tau') \\ & + \frac{NJ^2}{4} \int_{\tau,\tau'} \sum_{ab} Q_{ab}^{\circ 3}(\tau,\tau') - N \int_{\tau,\tau'} \sum_{ab} \Sigma_{ab}(\tau,\tau') G_{ab}(\tau,\tau') \\ & - \frac{N}{2} \int_{\tau,\tau'} \sum_{ab} \Pi_{ab}(\tau,\tau') Q_{ab}(\tau,\tau') \end{aligned} \tag{10}$$

Here, $\int_{\tau,\tau'}$ is shorthand for integration over τ, τ', and Tr is trace over both replica indicse and τ. In the above, replica indices a, b runs from 1 to r, and at the end of calculation, one need to take $r \to 0$ limit carefully. In the limit of large-N, the set of saddle point equations is given as follows:

$$\tilde{Q}_{ab}^{-1}(\omega_k) = (\omega_k^2/\Gamma + z)\, \delta_{ab} - \Pi_{ab}(\omega_k), \tag{11}$$

$$\Pi_{ab}(\tau) = \frac{3J^2}{2} Q_{ab}^2(\tau) + V^2 Q_{ab}^3(\tau) G_{ab}^4(\tau), \tag{12}$$

$$G_{ab}^{-1}(\omega_n) = -i\omega_n \delta_{ab} - \Sigma_{ab}(\omega_n), \tag{13}$$

$$\Sigma_{ab}(\tau) = V^2 Q_{ab}^4(\tau) G_{ab}^3(\tau). \tag{14}$$

Here, $\omega_k = 2k\pi k_B T$ and $\omega_n = (2n+1)\pi k_B T$ are bosonic and fermionic Matsubara frequencies, respectively, with $n, k \in \mathbb{Z}$ and k_B the Boltzmann constant. The parameter $\Gamma = \hbar^2/MJ$ controls quantum fluctuation. The functions $Q_{ab}(\tau)$ and $G_{ab}(\tau)$ are the order parameter fields or Green's functions for the bosonic and fermionic degrees

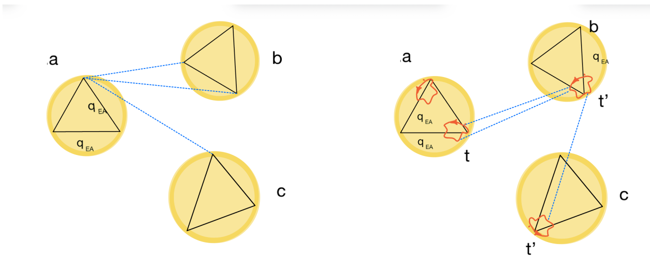

FIG. 2. Hierarchical (Parisi) structure of configurations. Left: classical. Within a state **a,b,c ...** almost all configurations are at the same distance from one another q_{EA}, a known property of high-dimensional sets. Similarly, the mutual distance between any two configurations in different states is also the same, but different from q_{EA} . Right: quantum. The situation is the same, but now we have a 'collar' of configurations, the imaginary-time trajectory, whose 'beads' are labeled by t. The organization now extends one step inwards: two different times of a trajectory are at the same distance from any time a trajectory in another state.

of freedom, respectively, defined as:

$$G_{ab}(\tau) = \frac{1}{N}\sum_i \langle \chi_{ia}(\tau)\chi_{ib}(0)\rangle, \tag{15}$$

$$Q_{ab}(\tau) = \frac{1}{N}\sum_i \langle s_{ia}(\tau)s_{ib}(0)\rangle. \tag{16}$$

The quantities $\Pi_{ab}(\tau)$ and $\Sigma_{ab}(\tau)$ represent the bosonic and fermionic self-energies in imaginary time, respectively. The Matsubara transforms of $Q_{ab}(\tau)$ are defined as:

$$\tilde{Q}_{ab}(\omega_k) = \int_0^{1/T} d\tau\, e^{i\omega_k\tau} Q_{ab}(\tau), \tag{17}$$

$$Q_{ab}(\tau) = T\sum_{\omega_k} e^{-i\omega_k\tau}\tilde{Q}_{ab}(\omega_k), \tag{18}$$

and similar expressions hold for $G_{ab}(\omega_n)$ and the self-energy functions.

B. Structure of order parameter for bosons and fermions

The Parisi ansatz for the order parameters of a quantum problem $Q_{ab}(\tau)$, $G_{ab}(\tau)$, where τ is the Matsubara time is shown in figure 2. As in any quantum problem, we may think of trajectories as a closed 'collar' with 'beads' of indices τ, living *within a state* in the energy landscape. A natural generalization of ultrametricity is that two "beads" from a given chain are at the same distance of each monomer of a chain in another state see Fig. 2. This is the same as saying that only diagonal terms Q_{aa} and G_{aa} may depend on τ. In particular, this means that G_{ab} necessarily is zero for $a \neq b$, because it concerns different fermions at equal times.

In what follows, we will consider both the replica-diagonal ansatz (i.e., $Q_{ab} = 0$ for $a \neq b$) and the one-step replica symmetry breaking (1-RSB) ansatz for Q_{ab}. The fermionic Green's function $G_{ab}(\tau)$ will be taken in a replica-diagonal form throughout, as explained above. Before analyzing the results for the fully coupled fermion–boson system, we briefly review the decoupled limit ($V = 0$) for the bosons, as well as the independent solution of the all-to-all coupled fermions governed by the SYK model.

1. Phase structure of decoupled boson

In the decoupled case, i.e., $V = 0$, the spherical quantum p-spin glass model (with $p = 3$) is well studied and is known to host a rich phase diagram [26]. The replica-diagonal Q_{aa} paramagnetic phase exists in the region of relatively high temperature and large quantum fluctuations Γ. Interestingly, the $p = 3$ model exhibits a particular temperature $T_p \approx 0.167$, below which two distinct paramagnetic solutions coexist within a finite range of the quantum parameter, $\Gamma_{c1} < \Gamma < \Gamma_{c2}$. They are now everywhere continuously connected, just like a liquid-gas transition. They prolong into two regimes: one at large quantum fluctuations ($\Gamma \gg 1$), referred to as the *quantum paramagnet*, and the other at small quantum fluctuations ($\Gamma \ll 1$), referred to as the *classical paramagnet*. For temperatures $T > T_p$, only a single paramagnetic solution exists for each value of Γ, and the classical and quantum paramagnetic regimes are smoothly connected.

At low temperatures, a one-step replica symmetry broken (1-RSB) spin-glass phase emerges. The bosonic order parameter in the 1-RSB phase takes the following form:

$$Q_{ab}(\tau) = (Q_d(\tau) - q_{\rm EA})\,\delta_{ab} + q_{\rm EA}\,\epsilon_{ab}, \tag{19}$$

where $\epsilon_{ab} = 1$ if replicas a and b belong to the same diagonal block, and $\epsilon_{ab} = 0$ otherwise. The parameter $q_{\rm EA}$ represents the off-diagonal component within the replica blocks and is known as the Edwards–Anderson (EA) order parameter.

Depending on how the replica symmetry breaking breakpoint parameter m is determined, two types of spin-glass phases can be distinguished: (a) *Thermodynamic spin glass:* The breakpoint m is determined by minimizing the free energy, ensuring thermodynamic stability. (b) *Marginal spin glass:* The breakpoint m is fixed by requiring that the replicon eigenvalue vanishes, leading to a marginally stable gapless solution. (This alternative has been advocated in Ref. [35] for quantum models, and has become widespread, but it has to be remembered that it does not correspond to thermal equilibrium) Referring to Figure 1, tuning the value of m between these points we capture metastable states ranging from the lowest, that dominate the thermodynamic measure, to the highest 'threshold states', which are gapless and are the ones that are relevant for most of the out of equilibrium situations.

2. Saddle point equation of pure SYK fermion

Here, we briefly review the saddle-point equations for the pure SYK model, whose Hamiltonian is given by Eq. (6). The coupling in the original SYK model has a random Gaussian-distribution with zero mean and finite standard deviation. In the large-N limit, the Schwinger-Dyson (saddle-point) equations for SYK model take the following form:

$$G^{-1}(\omega_n) = -\mathrm{i}\omega_n - \Sigma(\omega_n), \tag{20}$$

$$\Sigma(\tau) = \mathcal{J}^2 G^3(\tau), \tag{21}$$

where $G(\tau)$ is the fermionic Green's function, and $\Sigma(\tau)$ is the self-energy. In the low-energy or long-time limit, the derivative term $(-\mathrm{i}\omega_n)$ can be neglected, leading to a conformal (power-law) solution. Moreover, the saddle-point equations exhibit an emergent time-reparameterization symmetry under arbitrary transformations $\tau \to f(\tau)$ in this limit.

In our model, the fermionic saddle-point equations, given by Eqs. (13) and (14), can be comparable to the SYK saddle point equations 20 and 21 by interpreting an imaginary time dependent effective coupling as given by the form

$$\mathcal{J}_{\text{eff}}(\tau) = V \cdot Q^2(\tau),$$

where $Q(\tau)$ is the bosonic Green's function. The effective $\mathcal{J}_{\text{eff}}(\tau)$ encodes the fluctuating spin configuration of the quantum spin degrees of freedom. The explicit imaginary-time dependence of $\mathcal{J}_{\text{eff}}(\tau)$ explicitly breaks the time-reparameterization symmetry and therefore does not support conformal solutions in general. In the next section, we discuss the above time-dependent coupling in spin-glass phase in low temperatures can be effectively a static coupling, and we expect usual conformal invariant SYK Green's function in low temperatures.

III. COUPLED MODEL: THE SPIN-GLASS PHASE

In the glass phase we expect that the variables $\vec{s}$ are confined to pure states $\vec{s}^a$, where 'a' labels the states. Each is present with with a probability and an organization given by the Parisi ansatz. More generally, the system may find itself in metastable equilibrium in any metastable state, even those having relatively high free energies. As we have mentioned above, within a state a, the fermions feel an effective interaction $\mathcal{J}^{(a)}_{mnpq} \equiv \sum_{ijkl} V^{mnpq} s^a_i s^a_j s^a_k s^a_l$. For low enough temperature and sufficiently low Γ , one expects that each $\mathcal{J}^{(a)}_{mnpq}(t) \sim \sum_{ijkl} V^{mnpq} m^a_i m^a_j m^a_k m^a_l + \mathcal{J}^{fluctuating}_{mnpq}(t)$, where m^a_i are the expectations of the s_i within a state a $(\sum (m^a_i)^2 = q_{ea})$. The fluctuating part has zero expectation and short time correlation, except for the marginal (threshold) states(See Figure 1).

Consistently with the above picture, we find numerically that, in the classical limit $\Gamma \to 0$, the fermionic Green's function takes the form of that in the pure SYK model with a renormalized static coupling strength $\mathcal{J}^{(a)}_{\text{eff}}$. Furthermore, the feedback effect of fermions on the bosonic self-energy is negligible; as a result, the bosonic Green's function remains unchanged upon coupling.

In the following, we analyze the behavior of the bosonic and fermionic Green's functions in the glass phase for relatively large values of Γ. For strong quantum fluctuations ($\Gamma > 0$), tunneling between distinct pure states a and b can occur. At very low temperatures, the fermions predominantly experience the fluctuations of a single pure state a. At intermediate temperatures, however, where many (metastable) pure states become thermally accessible with appreciable probability within the Parisi hierarchical organization, the fermions effectively find a mixed environment arising from different pure states.

To this end, we present our results for the thermodynamic glass regime, followed by the results in the marginal glass phase. In the glass phase within the 1-RSB ansatz, the regular part of the bosonic correlator is defined as

$$Q_{\text{reg}}(\tau) = Q_{aa}(\tau) - q_{\text{EA}},$$

where q_{EA} is the off-diagonal Edwards–Anderson parameter.

We begin by examining how the Edwards–Anderson parameter q_{EA} and the associated break-point parameter m vary with temperature and coupling strength across different regions of the Γ–T phase diagram. We then turn to the effect of boson–fermion coupling on both the bosonic Green's function (regular part) and the fermionic Green's function.

A. Effect of fermion-boson coupling on phase diagram

First, we discuss the effect of fermion–boson coupling (V) on the breakpoint parameter m and the Edwards–Anderson parameter q_{EA}. The breakpoint m can take the values between 0 and 1. In the decoupled $p = 3$ spin-glass model (i.e.,the case with $V = 0$), the phase boundary between the spin-glass and paramagnetic phases is determined by the condition $m = 1$, which can be obtained either by thermodynamic stability criteria or via the marginal stability condition [26]. At this phase transition, the Edwards–Anderson parameter q_{EA} exhibits a discontinuous jump from a finite value to zero. As shown in Refs. [26, 48], increasing quantum fluctuations (i.e., increasing Γ) tends to suppress q_{EA} and destabilize the spin glass phase at large Γ.

In our coupled boson–fermion model, the equations determining m and q_{EA} retain the same structure as in the decoupled case ($V = 0$), as detailed in Appendix A. This is because the fermion–boson coupling term does not explicitly depend on the parameter m, owing to

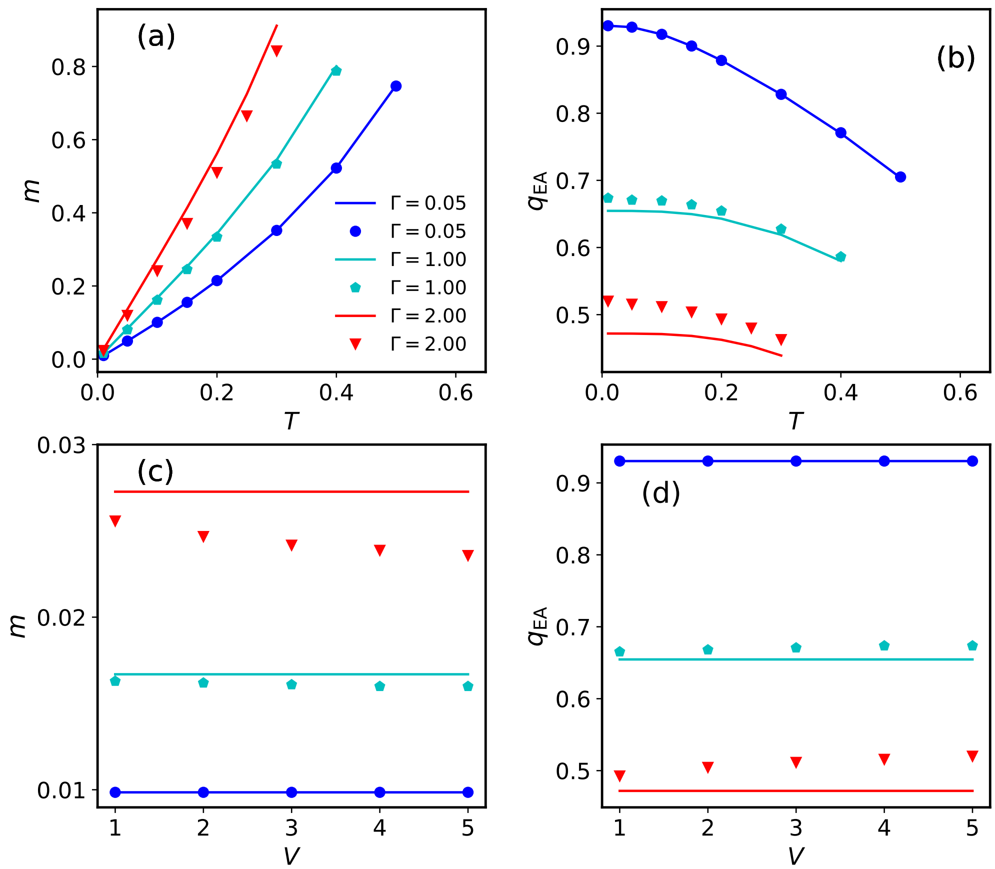

FIG. 3. **Effect of fermion-boson coupling on Edward-Anderson and break-point parameter:** Panels (a) and (b) show the breakpoint parameter m and the Edwards–Anderson parameter q_{EA}, respectively, as functions of temperature T for various values of the quantum fluctuation parameter Γ, with the coupling strength fixed at $V/J = 5$. Solid lines correspond to the decoupled spin-glass system, while markers indicate results from the fully coupled boson–fermion system. Panels (c) and (d) display m and q_{EA}, respectively, as functions of the boson–fermion coupling strength V (with $J = 1$), for the same values of Γ as in (a), at fixed temperature $T = 0.01$. As before, solid lines represent the decoupled case, and markers denote the fully coupled system.

the fact that the fermionic Green's function is diagonal, $G_{ab}(\tau) = G(\tau)\delta_{ab}$. The effect of the fermion–boson coupling enters the equations for m and q_{EA} only indirectly, through the local component of the spin correlator $Q_{aa}(\omega_k = 0)$, which is modified by the fermionic self-energy feedback on the bosons.

In Fig. 3(a) and (b), we show the breakpoint parameter m and the Edwards–Anderson parameter q_{EA}, respectively, as functions of temperature T for various values of the quantum parameter Γ, at fixed coupling strength $V/J = 5$. In Fig. 3(c) and (d), we present the corresponding behavior as functions of the boson–fermion coupling strength V (with $J = 1$), at fixed low temperature $T = 0.01$. In the Fig. 3, we determine m and q_{EA} using the thermodynamic stability criteria.

From these results, we observe that the coupling to fermions enhances q_{EA} and reduces the breakpoint parameter m. This effect becomes more pronounced at larger Γ, especially in the low-temperature regime. In the classical limit ($\Gamma \to 0$), we observe no change in either parameter. Since the phase boundary is defined by the condition $m = 1$, a reduction in m implies that the transition line into the spin-glass phase shifts to higher temperatures. These findings indicate that coupling to fermions tends to stabilize and promote the spin-glass phase for large values of Γ. We find similar qualitative results for marginal spin-glass phase.

B. Green's function in thermodynamic spin-glass phase

In Figure 4(a), (b), we plot the regular part of the bosonic Green's function, $Q_{\rm reg}(\tau) = Q_{aa}(\tau) - q_{\rm EA}$ for various values of temperature T. Panels (a) and (b) correspond to boson–fermion coupling strengths $V/J = 1.0$ and $V/J = 5.0$, respectively for quantum parameter $\Gamma = 2.0$. We obtain the result here using the thermodynamic spin-glass criterion. Each plots include both the Green's function for the decoupled case ($V = 0$), labeled as Q_0, and the fully coupled case, labeled as Q. The results are shown on a normal-log scale, with a linear x-axis and logarithmic y-axis, which allows us to examine the exponential decay behavior of the Green's function.

We observe that $Q_{0,\rm reg}(\tau)$ exhibits a linear profile on the semi-logarithmic scale over the interval $\tau \in [0, \beta/2)$, indicating an exponential decay of the form $Q_{0,\rm reg}(\tau) \sim e^{-E_g \tau}$ in this regime. This behavior show the presence of an energy gap E_g in the equilibrium spin-glass excitation spectrum, and consequently the low-temperature specific heat scaling $C_v \sim e^{-E_g/T}$ [26].

The effect of coupling on the bosonic Green's function can be summarized as follows. First, the value of $Q_{\rm reg}(\tau)$ near $\tau \sim \beta/2$ is significantly altered upon coupling to fermions, with the modification becoming more pronounced at lower temperatures. Second, the exponential decay of $Q_{\rm reg}(\tau)$ observed in the decoupled case over the interval $\tau \in [0, \beta/2)$ is replaced in the coupled system by a plateau-like behavior at intermediate times, characterized by much slower temporal variation. This qualitative change—from exponential decay to an approximate plateau—is induced by the fermionic self-energy feedback, which modifies the long-time structure of the bosonic Green's function and consequently changes the gap excitation spectrum of the equilibrium spin-glass phase. We note that this effect is already present for $V/J = 1$ (see panel (a)), increasing the coupling V/J mainly affects the range of temperatures where deviations become important.

In Figure 4(c) and (d), we show the fermionic Green's function $G(\tau)$ for various temperatures with the parameters same as those used in Figure 4(a) and (b) respectively. All plots are shown on a linear scale. The solid lines represent results from the fully coupled fermion–boson system, while the dotted lines correspond to the pure SYK Green's function computed with an effective renormalized static coupling $\mathcal{J}_{\rm eff} = V \cdot \langle Q^2(\tau)\rangle$, where the bosonic Green's function $Q(\tau)$ is replaced by its average value in the fermionic self-energy.

At very low temperatures, such as $T = 0.01$, the fermionic Green's function matches precisely with the SYK Green's function using the static renormalized coupling $\mathcal{J}_{\rm eff} = V \cdot \langle Q^2(\tau)\rangle$. This agreement can be attributed to the bosonic Green's function becoming nearly time-independent at low temperatures—i.e., $Q(\tau) \approx q_{\rm EA} + Q_{\rm reg}(\tau)$ with $Q_{\rm reg}(\tau)$ nearly constant—making the replacement by a constant average value a good approximation.

However, as the temperature increases, deviations between the full fermionic Green's function and the SYK Green's function with a renormalized static coupling become noticeable. This discrepancy is more pronounced at higher coupling strengths (e.g., $V/J = 5.0$). This behavior can be understood within the picture of pure-state organization in the Parisi scheme described earlier. At very low temperatures, the bosonic spins are confined to a specific pure state a, so the fermions effectively experience a static background interaction characterized by $\mathcal{J}_{\rm eff}^{(a)}$. In contrast, at intermediate temperatures, other metastable states acquire non-negligible statistical weight, and tunneling between different pure states in the spin-glass landscape becomes likely. Consequently, the fermions experience a state-mixing dynamic $\mathcal{J}_{\rm eff}(\tau)$ coupling environment, which leads to deviations from the pure SYK behavior with a static $\mathcal{J}_{\rm eff} = V \cdot \langle Q^2(\tau)\rangle$. This suggests the existence of a crossover temperature $T^*(V)$ separating a low temperature regime where the SYK fixed point is recovered from an intermediate one where significant deviations appear. As compared to a conventional SYK model, the Green's function in this phase decays faster at short-imaginary times while it slows down for $\tau \sim \beta/2$, possibly indicating a modification of the power-law behavior found in SYK.

Furthermore, in Appendix C, we present the power-law scaling of the fermionic Green's function and demonstrate how it is gradually modified as the temperature is increased to intermediate values.

C. Green's function in marginal spin-glass phase

Here, we present the results for the bosonic Green's function in the coupled problem, obtained under the marginal stability criterion. Marginal stability requires the replicon eigenvalue to vanish, selecting a flat direction in the free-energy functional, as illustrated in Fig. 1. In the decoupled p-spin glass model under this condition, the excitation spectrum is gapless critical behaviour and the regular part of the correlator exhibits a power-law decay, $Q_{0,\rm reg}(\tau) \sim 1/\tau^{\alpha}$ [26]. Consequently, the specific heat displays linear temperature dependence, $C_V \propto T$ [26].

Figure 5(a) shows the bosonic Green's function $Q_{\rm reg}(\tau)$ for the coupled system and $Q_{0,\rm reg}(\tau)$ for the decoupled case as functions of τ/β up to $\tau = \beta/2$, plotted on a log–log scale. The inset presents the full profiles of both correlators on a semi-logarithmic scale (logarithmic y-axis). These results are shown for $V/J = 5.0$ and $\Gamma = 2.0$. As is evident from the figure, coupling to fermions shortens the power-law regime (linear segment in the log–log plot) at $\tau < \beta/2$ and leads to the development of a slowly varying plateau near $\tau \sim \beta/2$.

The corresponding fermionic Green's function for the coupled system, along with its comparison to the pure SYK Green's function with a static renormalized cou-

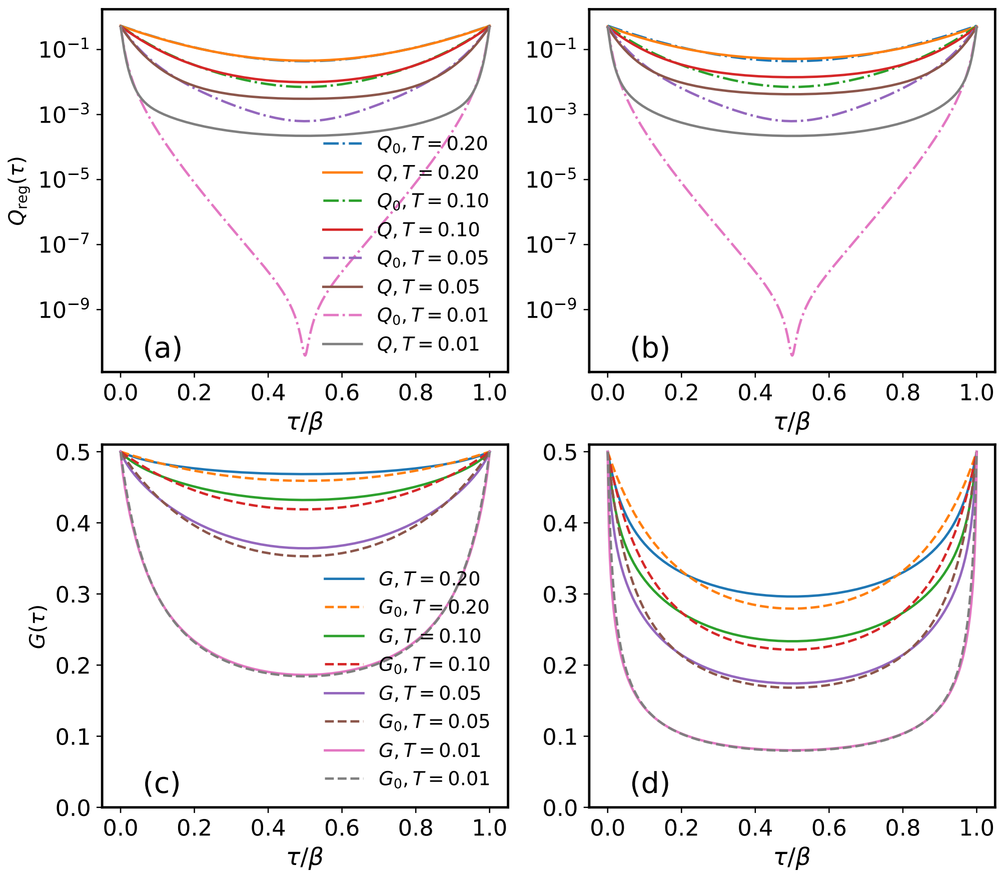

FIG. 4. **Upper panel (a, b) — Bosonic Green's function:** The regular part of the bosonic Green's function, defined as $Q_{\rm reg}(\tau) = Q_{aa}(\tau) - q_{\rm EA}$, is plotted as a function of τ/β for various temperatures T. Panel (a) corresponds to quantum fluctuation parameter $\Gamma = 2.0$ and coupling strength $V/J = 1.0$, while panel (b) shows results for $V/J = 5.0$. In the legend, Q_0 denotes the bosonic Green's function in the absence of fermion–boson coupling ($V = 0$), and Q corresponds to the fully coupled case ($V \neq 0$). These results are for thermodynamic spin-glass case. **Lower panel (c, d) — Fermionic Green's function:** The corresponding fermionic Green's functions are shown in panels (c) and (d), with parameters matching those in (a) and (b), respectively. In the legend, G represents the fermionic Green's function of the fully coupled boson–fermion system, and G_0 refers to the SYK Green's function computed with a renormalized effective coupling $\mathcal{J}_{\rm eff} = V \cdot \langle Q^2(\tau)\rangle$.

pling, is shown in Fig. 5(b). Its behavior closely parallels that observed in Fig. 4(d) for the thermodynamic glass phase.

D. Wavefunctions

Although we shall not make a detailed analysis of this here, we may guess what the wavefunctions look like at very low temperatures, and not too high values of Γ. Consistently with the discussion above, an approximate set of eigenvalues of the pure boson term is constructed with the lowest eigentates $|\alpha; a\rangle$ concentrated around each minimum s^a, where α are quantum numbers. The lowest fermionic eigenstates within this state correspond to an effective SYK model with effective couplings $\mathcal{J}^{(a)}_{mnpq}$. The set of eigenstates living in the metastable state a are then constructed as combinations of tensor products of these two sets. Eigentsates corresponding to different valleys are orthogonal both because their bosonic functions are, but also because the fermionic effective interactions $\mathcal{J}^{(a)}_{mnpq}$ that gave rise to them are very different. A better analysis may be done either by considering the real-time dynamics starting in various places, or the 'Franz-Parisi construction', which still needs to be developed for quantum systems.

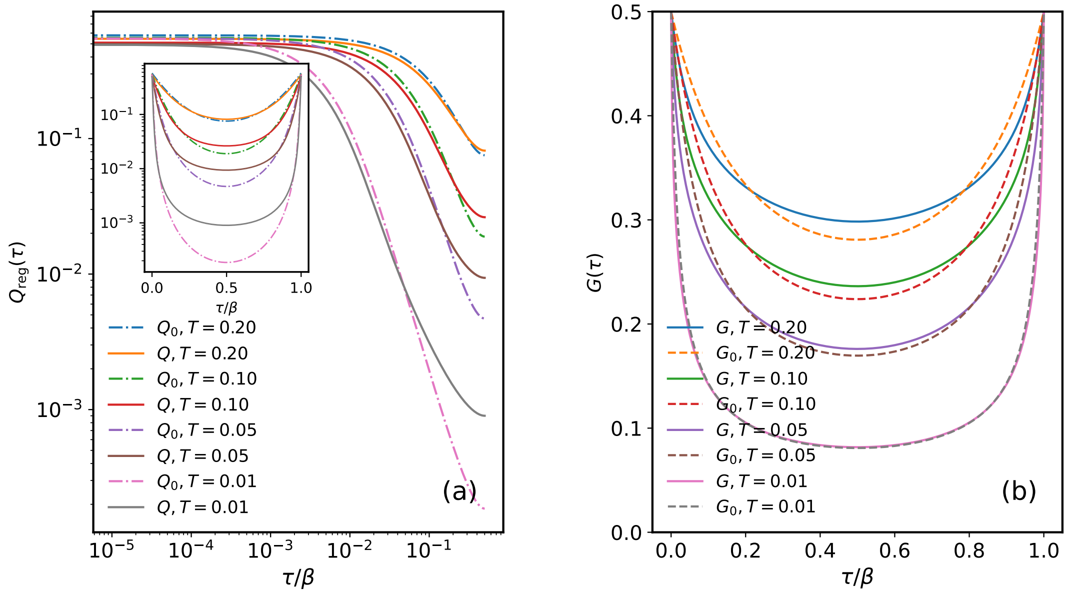

FIG. 5. **Left panel (a) — Bosonic Green's function:** The regular part of the bosonic Green's function is plotted as a function of τ/β (upto $\tau = \beta/2$) for different T in log-log scale in panel (a). The result corresponds to $\Gamma = 2.0$ and coupling strength $V/J = 5.0$. In the legend, Q_0 denotes the bosonic Green's function in the absence of fermion–boson coupling ($V = 0$), and Q corresponds to the fully coupled case ($V \neq 0$). These results are for **marginal spin-glass case**. In the inset, the results are shown in semi-logarithmic scale (y-axis) to show the full $Q(\tau)$ vs τ/β profile. **Right panel (b) — Fermionic Green's function:** The corresponding fermionic Green's functions are shown in panel (b) with parameters matching those in (a). In the legend, G represents the fermionic Green's function of the fully coupled boson–fermion system, and G_0 refers to the pure SYK Green's function computed with a static renormalized effective coupling $\mathcal{J}_{\rm eff} = V \cdot \langle Q^2(\tau)\rangle$.

IV. COUPLED MODEL: PARAMAGNETIC PHASE

In this section, we discuss how the fermion-boson coupling in the paramagnetic phase affects the bosonic and fermion Green's function.

A. Quantum paramagnet

In Figure 6 (a) and (b), we present the bosonic Green's function $Q(\tau)$ for the coupled system ($V \neq 0$) at several values of the quantum parameter $\Gamma = 3.0,\ 3.5,\ 4.0$ corresponding to the quantum paramagnetic solutions. Panels (a) and (b) correspond to boson–fermion coupling strengths $V/J = 2.0$ and $V/J = 5.0$, respectively, computed at temperature $T = 0.125$. These plots are presented on a semi-logarithmic scale with logarithmic y-axis. In each case, we compare the results with those from the decoupled system ($V = 0$), denoted as $Q_0(\tau)$.

In the quantum paramagnetic phase, the bosonic Green's function exhibits exponential decay over the interval $\tau \in [0, \beta/2]$, as evidenced by the clear linear behavior in the semi-logarithmic plots. This exponential decay corresponds to a gapped spectral function in the real-frequency domain. Upon coupling to fermions, we observe that the value of $Q(\tau)$ near $\tau \sim \beta/2$ is only mildly affected, and the exponential decay characteristic of the quantum paramagnetic phase is largely preserved.

The corresponding fermionic Green's functions for the same parameters as in Figure 6 (a) and (b) are shown in panels (c) and (d), respectively, plotted on a linear scale. We find that the fermionic Green's function exhibits a rapid initial decay followed by a plateau at intermediate times, with $G(\tau \sim \beta/2) < 0.5$. The plateau value decreases with increasing coupling strength V/J, and for a fixed V/J, it further decreases with decreasing Γ.

We emphasize that this is a rather surprising result, since naively one could have expected that coupling the SYK with a gapped phase as the quantum paramagnet should not lead to significant renormalization. Instead our results show that the parametric coupling between fermions and gapped bosons can lead to a complete restructuring of the fermionic dynamics. Furthermore, the nature of the resulting slow fermionic dynamics contrasts markedly with that of the SYK model in the limit of vanishing coupling $\mathcal{J} \to 0$, as well as with free Majorana fermions, for which the Green's function takes the simple form $G(\tau) = \frac{1}{2}\,\mathrm{sign}(\tau)$. The Green's function for the pure SYK model in the $\mathcal{J} \to 0$ limit is presented in Appendix B. It is tempting to speculate that the observed slow dynamics for the fermions arises from noisy effective couplings induced by the disordered spins, leading to an effective model reminiscent of a brownian SYK [49–51].

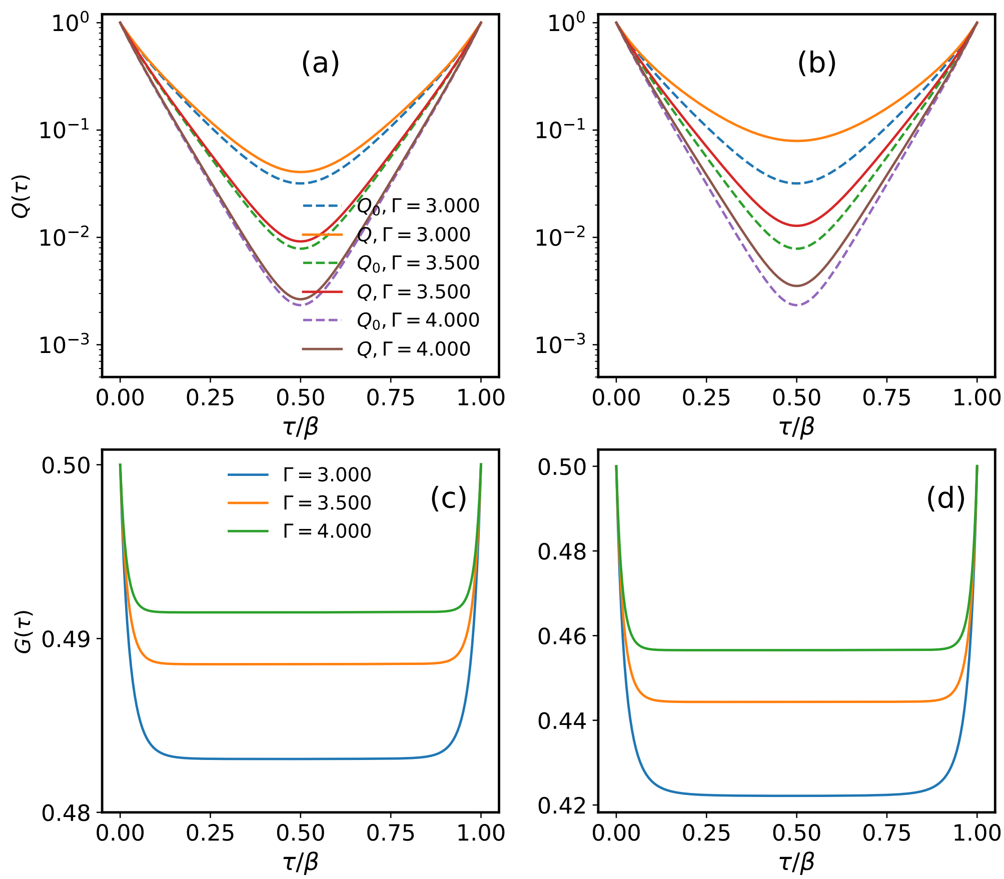

FIG. 6. **Upper panel (a, b) — Bosonic Green's function:** The bosonic Green's function $Q(\tau)$ is shown for several values of the quantum fluctuation parameter Γ in the quantum paramagnetic phase at $T = 0.125$. Panel (a) corresponds to boson–fermion coupling strength $V/J = 2.0$, while panel (b) shows results for $V/J = 5.0$. The curve labeled Q_0 represents the bosonic Green's function in the decoupled case ($V = 0$). **Lower panel (c, d) — Fermionic Green's function:** The corresponding fermionic Green's functions for the coupled boson–fermion system are displayed in panels (c) and (d), using the same parameters as in panels (a) and (b), respectively.

B. Classical paramagnet

In Figure 7 (a), we present the bosonic Green's function $Q(\tau)$ for several values of the quantum parameter $\Gamma = 2.0,\ 3.0,\ 3.5$ corresponding to classical paramagnetic solutions at temperature $T = 0.125$. The plot is shown on a linear scale, and the boson–fermion coupling strength is fixed at $V/J = 2.0$. For comparison, we also show the decoupled case ($V = 0$), denoted as $Q_0(\tau)$. These solutions are termed *classical paramagnetic* since the mid-point value $Q(\tau = \beta/2)$ is much larger than in the quantum paramagnetic solutions presented in Figure 6. The classical paramagnet is characterized by an early decay in τ, followed by a plateau at value q_P. The coupling to fermions has only a minimal effect on the plateau value q_P for $V/J = 2.0$, and the deviation becomes more noticeable at stronger coupling (result not presented here).

The corresponding fermionic Green's functions $G(\tau)$ are displayed in Figure 7 (b) for the same parameters as in panel (a). The fermionic Green's function closely matches the pure SYK Green's function computed using an effective coupling $\mathcal{J}_{\text{eff}} = V \cdot q_P^2$, where q_P is the plateau value of $Q(\tau)$ from panel (a). This indicates that, in the classical paramagnetic regime, coupling to fermions does not qualitatively alter the behavior of either the bosonic or fermionic Green's functions.

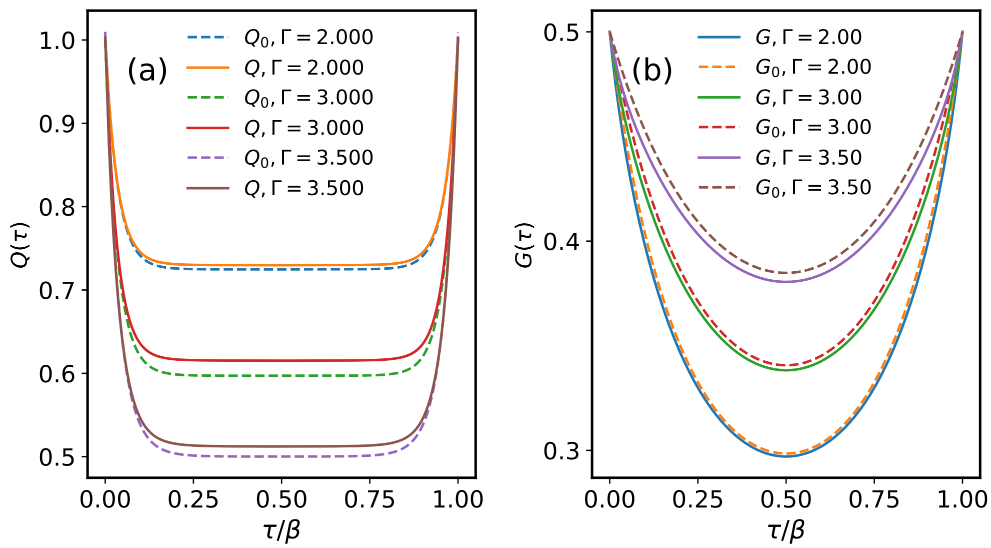

FIG. 7. (a) The classical paramagnetic solutions are shown for different values of the quantum parameter Γ at fixed temperature $T = 0.125$. Both the decoupled (Q_0) and coupled (Q) bosonic Green's functions are plotted for comparison. The boson–fermion coupling strength is set to $V/J = 2.0$. (b) The corresponding fermionic Green's functions are displayed. Here, G represents the full numerical solution for the coupled system, while G_0 denotes the pure SYK Green's function with an effective coupling $J_{\text{eff}} = V \cdot q_P^2$, where q_P is the plateau value of $Q(\tau)$ from panel (a).

V. CONCLUSION AND DISCUSSION

In this work, we studied a model of disordered fermion–boson interactions, where Majorana fermions interact via all-to-all random four-fermion couplings as in the SYK model, and are simultaneously coupled to bosonic degrees of freedom governed by a quantum spherical $p = 3$ spin-glass model. The bosonic sector features a rugged free energy landscape and exhibits a spin-glass phase at low temperatures characterized by a one-step replica symmetry breaking (1-RSB) structure, and a paramagnetic phase at large quantum fluctuations ($\Gamma \gg 1$) or high temperature.

The fermions, evolving within the valleys of this complex landscape, experience effective couplings that depend sensitively on the organization of pure states in the Parisi scheme. When the bosonic density matrix is dominated by a single pure state, the fermions effectively experience a static, renormalized coupling of the form $\mathcal{J}^{(a)}_{mnpq} = \sum_{ijkl} V^{mnpq}_{ijkl} s^{(a)}_i s^{(a)}_j s^{(a)}_k s^{(a)}_l$. In contrast, when multiple pure states contribute significantly, the fermions encounter a dynamic, state-mixing coupling in imaginary time. Our large-N saddle-point analysis supports this intuitive picture: in the spin-glass phase, the fermionic Green's function follows the SYK form at low temperatures, while deviations from this behavior appear at higher temperatures due to dynamical mixing.

The feedback of fermions on the bosonic sector is equally striking. In the decoupled limit, the bosonic Green's function decays exponentially in the equilibrium spin-glass phase and as a power law in the marginal spin-glass regime. Upon coupling to fermions, both behaviors are replaced by a slowly varying, plateau-like profile in imaginary time, signaling a qualitative shift in bosonic dynamics. In the paramagnetic phase, however, the bosonic Green's function remains largely unaffected—retaining its plateau-like structure in the classical regime ($\Gamma \ll 1$) and exponential decay in the quantum regime ($\Gamma \gg 1$). The fermionic sector, by contrast, displays rich behavior: in the classical paramagnetic regime, it remains well described by the SYK form upon coupling, whereas in the quantum paramagnetic regime, it departs significantly from the SYK behavior and instead develops a plateau-like structure.

Overall, our results demonstrate how disordered fermion–boson coupling qualitatively modifies both bosonic and fermionic correlators, revealing a crossover from SYK-like behavior at low temperatures to distinctly non-SYK behavior in the paramagnetic regime dominated by strong quantum fluctuations.

An interesting direction for future exploration concerns the out-of-equilibrium dynamics of this coupled system. The relaxation dynamics of quantum glasses has been extensively studied both in presence of dissipation and under unitary dynamics [52–57]. When the bosonic sector is connected to a zero-temperature bath, it is known to exhibit aging: the system evolves increasingly slowly without ever equilibrating. In this setting, the effective fermionic couplings $\mathcal{J}_{mnpq}$ become slowly time-dependent, mirroring the aging of the bosons. Since the bosonic fluctuations are governed by an effective temperature $T_{\rm eff} > 0$ [25], the fermions inherit this effective temperature and never fully reach a zero-temperature state as long as the system remains out of equilibrium. This behavior would be therefore in stark contrast with the dynamics of a pure SYK model which instead displays fast thermalization [58–63].

Understanding the consequences of such aging dynamics on the fermionic sector and more broadly, on the interplay between quantum chaos and glassiness remains a compelling question for future study.

VI. ACKNOWLEDGEMENTS

S.B. and M.S. acknowledge funding from the European Research Council (ERC) under the European Union's Horizon 2020 research and innovation program (Grant agreement No. 101002955 – CONQUER). We acknowledge Collège de France IPH cluster where the numerical calculations were carried out.

Appendix A: Derivation of saddle point equations

To compute the disorder average free energy $F = -k_B T\overline{\log Z}$, we use the replica trick as follows:

$$\log Z = \lim_{r\to 0}\frac{Z^r - 1}{r} \tag{A1}$$

The replicated partition function of the Hamiltonian in eqn. 1 is given as follow:

$$Z^r = \int \mathcal{D}[s_a, \chi_a] e^{-S} \tag{A2}$$

where the imaginary time action S is given by:

$$\begin{aligned} S = \frac{1}{2}\int d\tau \sum_{m,a}\chi_{ma}(\tau)\partial_\tau\chi_{ma}(\tau) + \int d\tau \Bigg(\sum_{i,a}\frac{M}{2}\left(\frac{\partial s_{ia}}{\partial\tau}\right)^2 + \sum_{ijk,a} J_{ijk}s_{ia}(\tau)s_{ja}(\tau)s_{ka}(\tau)\Bigg) \\ + \int d\tau \sum_{ijkl;mnpq,a} V_{ijkl;mnpq}s_{ia}(\tau)s_{ja}(\tau)s_{ka}(\tau)s_{la}(\tau)\chi_{ma}(\tau)\chi_{na}(\tau)\chi_{pa}(\tau)\chi_{qa}(\tau) \end{aligned} \tag{A3}$$

In the above $a \in [1, r]$ is replica indices. In the end we take analytical continuation of $r \to 0$. Performing disorder average on $V_{ijkl;mnpq}$ yields:

$$\begin{aligned} &\prod_{i<j<k<l}^{m<n<p<q}\int dV_{ijkl;mnpq}\exp\left[-\frac{V^2_{ijkl;mnpq}}{2\sigma^2} - V_{ijkl;mnpq}\int d\tau\sum_a s_{ia}...s_{la}\chi_{ma}...\chi_{qa}\right] \\ &= \exp\left[\frac{NV^2}{4}\int d\tau d\tau'\sum_{ab}\left(\frac{1}{N}\sum_i s_{ia}(\tau)s_{ib}(\tau')\right)^4\left(\frac{1}{N}\sum_m\chi_{ma}(\tau)\chi_{mb}(\tau')\right)^4\right] \end{aligned} \tag{A4}$$

Similarly, we can perform the disorder average for J_{ijk} for $p = 3$ spin-glass part and we obtain:

$$\exp\left[-\int d\tau\sum_{ia}s_{ia}\big(-\frac{M}{2}\partial_\tau^2 + \frac{z}{2}\big)s_{ia}(\tau) + \frac{NJ^2}{4}\int d\tau d\tau'\sum_{ab}\left(\frac{1}{N}\sum_i s_{ia}(\tau)s_{ib}(\tau')\right)^3\right] \tag{A5}$$

where z is the Lagrange multiplier to enforce the spherical constraint. We introduce following large-N dynamical fields

$$G_{ab}(\tau,\tau') = \frac{1}{N}\sum_i\chi_{ia}(\tau)\chi_{ib}(\tau') \tag{A6}$$

$$Q_{ab}(\tau,\tau') = \frac{1}{N}\sum_i s_{ia}(\tau)s_{ib}(\tau') \tag{A7}$$

and we obtain disorder-average replicated partion function in terms of the above dynamical fields as follows:

$$\begin{aligned} \overline{Z^r} = \int\mathcal{D}[s,\chi]\exp\Bigg[-\int d\tau\frac{1}{2}\sum_{m,a}\chi_{ma}(\tau)\partial_\tau\chi_{ma}(\tau) + \frac{NV^2}{4}\int d\tau d\tau'\sum_{ab}Q^{\circ 4}_{ab}(\tau,\tau')G^{\circ 4}_{ab}(\tau,\tau') \\ - \int d\tau\sum_{ia}s_{ia}\big(-\frac{M}{2}\partial_\tau^2 + \frac{z}{2}\big)s_{ia}(\tau) + \frac{NJ^2}{4}\int d\tau d\tau'\sum_{ab}Q^{\circ 3}_{ab}(\tau,\tau')\Bigg]\delta\Big(NQ_{ab} - \sum_i s_{ia}s_{ib}\Big)\delta\Big(NG_{ab} - \sum_i\chi_{ia}\chi_{ib}\Big) \end{aligned} \tag{A8}$$

To promote G, Q as fluctuating dynamic fields, conjugate fields are introduced by using the relation $\delta\big(NG_{ab}(\tau,\tau') - \sum_m \chi_{ma}(\tau)\chi_{mb}(\tau')\big) = \int \mathcal{D}[\Sigma(\tau,\tau')]\exp[+\int d\tau d\tau' \Sigma_{ab}(\tau,\tau')\big(NG_{ab}(\tau,\tau') - \sum_m \chi_{ma}(\tau)\chi_{mb}(\tau')\big)]$ for $G_{ab}(\tau,\tau')$ and similarly for $Q_{ab}(\tau,\tau')$, $\delta\big(NQ_{ab}(\tau,\tau') - \sum_i s_{\gamma a}(\tau)s_{ib}(\tau')\big) = \int \mathcal{D}[\Pi(\tau,\tau')]\exp[-\int d\tau d\tau'(\Pi_{ab}(\tau,\tau')/2)\big(NQ_{ab}(\tau,\tau') - \sum_i s_{ia}(\tau)s_{ib}(\tau')\big)]$, where $\Pi(\tau,\tau')$ as the conjugate field. Next, we integrate over s, χ and get:

$$\overline{Z^r} = \int \mathcal{D}[G,\Sigma,Q,\Pi] e^{-S_{\text{eff}}[G,\Sigma,Q,\Pi]} \tag{A9}$$

The effective action S_{eff} reads as:

$$\begin{aligned} S_{\text{eff}} = {} & -N\,\mathrm{Tr}\ln\big(-G^{-1}_{0,ab} + \Sigma_{ab}\big) - \frac{N}{2}\mathrm{Tr}\ln\big(Q^{-1}_{0,ab} - \Pi_{ab}\big) + \frac{NV^2}{4}\sum_{ab}\int d\tau d\tau' G^{\circ 4}_{ab}(\tau,\tau')Q^{\circ 4}_{ab}(\tau,\tau') \\ & - N\int d\tau d\tau' \sum_{ab}\Sigma_{ab}(\tau,\tau')G_{ab}(\tau,\tau') - \frac{N}{2}\int d\tau d\tau' \sum_{ab}\Pi_{ab}(\tau,\tau')Q_{ab}(\tau,\tau') + \int d\tau d\tau' \frac{J^2}{4}\sum_{ab} Q^{\circ 3}_{ab}(\tau,\tau') \end{aligned} \tag{A10}$$

where

$$G^{-1}_{0,ab} = -\partial_\tau \delta(\tau-\tau')\delta_{ab} \tag{A11}$$

$$Q^{-1}_{0,ab} = \big(-\frac{1}{\Gamma}\partial^2_\tau + z\big)\delta(\tau-\tau')\delta_{ab} \tag{A12}$$

In the above derivation, we have set $\hbar = 1$, and introduced a quantum parameter $\Gamma = 1/MJ$. Taking the variation of S_{eff} with respect to $X(= G, Q, \Sigma, \Pi)$ and setting $\partial S_{\text{eff}}/\partial X_{ab} = 0$, we get:

$$Q^{-1}_{ab}(\tau,\tau') = Q^{-1}_0(\tau,\tau')\delta_{ab} - \Pi_{ab}(\tau,\tau') \tag{A13}$$

$$\Pi_{ab}(\tau,\tau') = \frac{3J^2}{2}Q^2_{ab}(\tau,\tau') + V^2 Q^3_{ab}G^4_{ab}(\tau,\tau') \tag{A14}$$

$$G^{-1}_{ab}(\tau,\tau') = G^{-1}_0(\tau,\tau')\delta_{ab} - \Sigma_{ab}(\tau,\tau') \tag{A15}$$

$$\Sigma_{ab}(\tau,\tau') = V^2 Q^4_{ab}(\tau,\tau')G^3_{ab}(\tau,\tau') \tag{A16}$$

1. Coupled Model: Paramagnetic phase

As discussed in the main text, the fermionic Green's function always takes the diagonal form:

$$G_{ab}(\tau) = G(\tau)\delta_{ab} \tag{A17}$$

and the bosonic Green's function (Q) has diagonal form in paramagnetic phase:

$$Q_{ab}(\tau) = Q(\tau)\delta_{ab} \tag{A18}$$

In this case, the saddle point equations become:

$$Q^{-1}(\tau) = Q^{-1}_0(\tau) - \Pi(\tau) \tag{A19}$$

$$\Pi(\tau) = \frac{3J^2}{2}Q^2(\tau) + V^2 Q^3(\tau)G^4(\tau) \tag{A20}$$

$$G^{-1}(\tau) = G^{-1}_0(\tau) - \Sigma(\tau) \tag{A21}$$

$$\Sigma(\tau) = V^2 Q^4(\tau)G^3(\tau) \tag{A22}$$

2. Coupled Model: Spin-glass phase

As before, the fermionic Green's function takes the diagonal form:

$$G_{ab}(\tau) = G(\tau)\delta_{ab} \tag{A23}$$

and the bosonic Green's function (Q) takes the 1-RSB form:

$$Q_{ab}(\tau) = (Q_d(\tau) - q_{\rm EA})\delta_{ab} + q_{\rm EA}\epsilon_{ab} \tag{A24}$$

where $\epsilon_{ab} = 1$ for a, b in diagonal block, otherwise it is zero. Here, $Q_d(\tau) = Q_{aa}(\tau)$ is diagonal component. In this case, the saddle-point equations become:

$$Q^{-1}_{ab}(\tau) = Q^{-1}_0(\tau)\delta_{ab} - \Pi_{ab}(\tau) \tag{A25}$$

$$\Pi_{ab}(\tau) = \frac{3J^2}{2}Q^2_{ab}(\tau) + V^2 Q^3_{ab}(\tau)G^4(\tau)\delta_{ab} \tag{A26}$$

$$G^{-1}(\tau) = G^{-1}_0(\tau) - \Sigma(\tau) \tag{A27}$$

$$\Sigma(\tau) = V^2 Q^4_{aa}(\tau)G^3(\tau) \tag{A28}$$

To write down explicitly the saddle point equations for Q_{ab} for $a = b$ and $a \neq b$, we write the above 1-RSB order parameter in Matsubara frequency:

$$\tilde{Q}_{ab}(\omega_k) = (\tilde{Q}_d(\omega_k) - \tilde{q}_{\rm EA})\delta_{ab} + \tilde{q}_{\rm EA}\epsilon_{ab}, \tag{A29}$$

where $\tilde{q}_{\rm EA} = \beta q_{\rm EA}\delta_{\omega_k,0}$ and $\tilde{Q}_d(\omega_k)$ is Matsubara Fourier transformation of $Q_d(\tau) = Q_{aa}(\tau)$. Now, it is convenient to write $Q_d(\tau) = Q_{\rm reg}(\tau) + q_{\rm EA}$. The inverse matrix $\tilde{Q}^{-1}(\omega_k)$ has the following structure [26]

$$\left(\tilde{Q}^{-1}\right)_{ab}(\omega_k) = A(\omega_k)\delta_{ab} + B(\omega_k)\epsilon_{ab} \tag{A30}$$

with

$$A(\omega_k) = \frac{1}{\tilde{Q}_d(\omega_k) - \tilde{q}_{\rm EA}}, \qquad B(\omega_k) = \frac{-\tilde{q}_{\rm EA}}{\tilde{Q}_d(\omega_k)^2 - (m-1)\tilde{q}^2_{\rm EA} + (m-2)\tilde{Q}_d(\omega_k)\tilde{q}_{\rm EA}}. \tag{A31}$$

Here, m is the break point and the above result for $A(\omega_k), B(\omega_k)$ is obtained after taking the replica limit $r \to 0$. The diagonal element of the inverse matrix $(\tilde{Q}^{-1})$ is given by

$$(\tilde{Q}^{-1})_{aa}(\omega_k) = A(\omega_k) + B(\omega_k) = \frac{\tilde{Q}_d(\omega_k) + (m-2)\tilde{q}_{\rm EA}}{(\tilde{Q}_d(\omega_k)^2 + (m-2)\tilde{q}_{\rm EA}\tilde{Q}_d(\omega_k) - (m-1)\tilde{q}^2_{\rm EA})}. \tag{A32}$$

The off-diagonal element ($a \neq b$) is

$$\left(\tilde{Q}^{-1}\right)_{ab}(\omega_k) = B(\omega_k). \tag{A33}$$

The saddle-point equation for diagonal component $\tilde{Q}_d(\omega_k)$ can be obtained by using equations (A25) and (A32) as

$$M\omega_k^2 + z = \frac{\tilde{Q}_d(\omega_k) + (m-2)\tilde{q}_{\rm EA}}{(\tilde{Q}_d(\omega_k)^2 + (m-2)\tilde{q}_{\rm EA}\tilde{Q}_d(\omega_k) - (m-1)\tilde{q}^2_{\rm EA})} + \Pi(\omega_k), \tag{A34}$$

with $\Pi(\omega_k) = \Pi_{aa}(\omega_k)$ is the Fourier transform of $\Pi_{aa}(\tau)$ which reads as:

$$\Pi_{aa}(\tau) = \frac{3J^2}{2}Q^2_d(\tau) + V^2 Q^3_d(\tau)G^4(\tau) \tag{A35}$$

The saddle point equation for $q_{\rm EA}$ is obtained using eqn.A33 and eqn.A26

$$0 = -\frac{q_{\rm EA}}{\tilde{Q}_d(0)^2 - (m-1)\beta^2 q^2_{\rm EA} + (m-2)\beta\tilde{Q}_d(0)q_{\rm EA}} + \frac{p}{2}q^{p-1}_{\rm EA}. \tag{A36}$$

Using eqn. A36, we can write down the diagonal saddle point equation more conveniently with $Q_{\rm reg}(\omega_k)$. This reads as:

$$M\omega_k^2 + z = \frac{1}{Q_{\rm reg}(\omega_k)} + \Pi_{\rm reg}(\omega_k) \tag{A37}$$

where

$$\Pi_{\rm reg}(\tau) = \frac{3J^2}{2}Q^2_d(\tau) + V^2 Q^3_d(\tau)G^4(\tau) - \frac{3J^2}{2}q^2_{\rm EA} \tag{A38}$$

Thermodynamic spin-glass phase and marginal spin-glass phase

In the thermodynamic spin-glass phase, the breakpoint parameter m is treated as a variational parameter that minimizes the free-energy functional. The value of m is determined by explicitly considering the m-dependence of the free-energy functional $f[m]$. The boson–fermion coupling term

$$\frac{NV^2}{4}\sum_{ab}\int d\tau d\tau'\, G_{ab}^{\circ 4}(\tau,\tau')\, Q_{ab}^{\circ 4}(\tau,\tau') \propto r\cdot \frac{NV^2}{4}\int d\tau d\tau'\, G^{\circ 4}(\tau,\tau')\, Q_{d}^{\circ 4}(\tau,\tau')$$

reduces to a term proportional to the replica index r because $G_{ab}(\tau) = G(\tau)\delta_{ab}$ is diagonal in replica space. As a result, this contribution doesnot depend on m, and the variation of $f[m]$ reproduces the same set of equations as in the decoupled ($V = 0$) p-spin-glass model. We refer the reader to Ref. [26] for a detailed derivation of these equations. For $p = 3$, the equation for m relating it to the Edwards–Anderson parameter q_{EA} is given by

$$\frac{p(\beta m)^2}{2}\, q_{\mathrm{EA}}^{p} = \frac{2x_p^2}{1+x_p}, \tag{A39}$$

where $x_p = \frac{my}{1-y}$, $y = \frac{\beta q_{\mathrm{EA}}}{\tilde{Q}_d(0)}$, is determined by

$$\ln\left(\frac{1}{1+x_p}\right) + \frac{x_p}{1+x_p} + \frac{x_p^2}{p(1+x_p)} = 0. \tag{A40}$$

For $p = 3$, it yields $x_p = 1.81696$.

In the marginal spin-glass phase, the breakpoint parameter m is determined by imposing the marginality condition, which requires the replicon eigenvalue $\Lambda_T = 0$. To compute the replicon eigenvalue, one considers the second-order variation of the free-energy functional with respect to Q_{ab} for $a \neq b$. For the same reason discussed in the thermodynamic spin-glass case, the boson–fermion coupling term does not modify the replicon eigenvalue which is given by[26]:

$$\Lambda_T = \beta^2\left[\frac{1}{\tilde{Q}_d(0)-\tilde{q}_{\mathrm{EA}}} - \frac{p(p-1)}{2} q_{\mathrm{EA}}^{p-2}\right] \tag{A41}$$

Consequently, the marginality condition remains identical to that of the decoupled case. In the marginal spin-glass phase, by setting $\Lambda_T = 0$, one obtain $x_p = p-2$, and the relation between m and q_{EA} is the same as given in Eq. A39.

Appendix B: The SYK Green's function for $\mathcal{J} \to 0$ limit

In Fig. 8, we present the pure SYK Green's function $G_0(\tau)$ as a function of τ for $T = 0.125$ and several small coupling strengths $\mathcal{J} = 0.2, 0.1, 0.05, 0.01$. As the coupling strength $\mathcal{J} \to 0$, $G_0(\tau)$ smoothly approaches the free-fermion Green's function, $G(\tau) = \frac{1}{2}\,\mathrm{sign}(\tau)$, as expected.

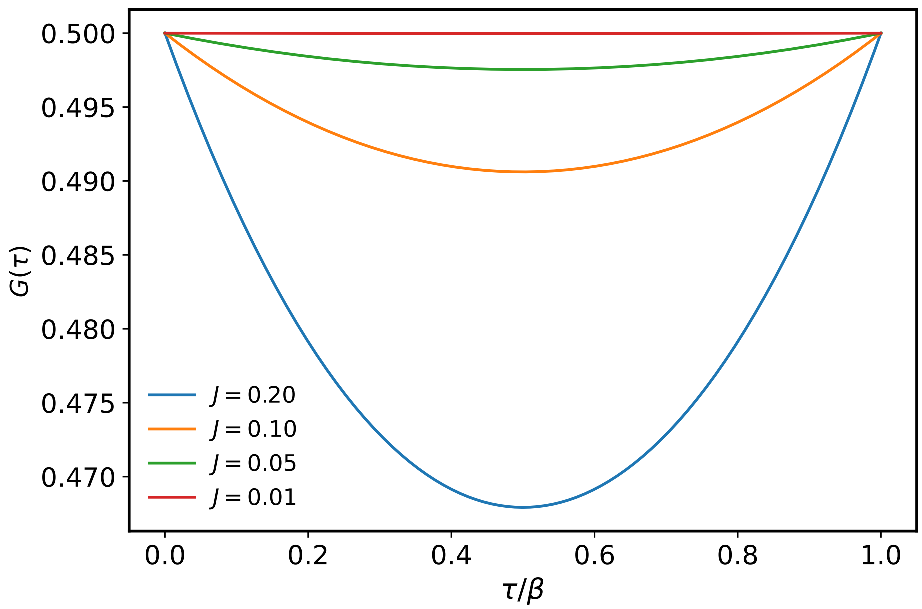

FIG. 8. The pure SYK Green's function $G(\tau)$ for coupling strength $\mathcal{J} = 0.2, 0.1, 0.01, 0.05$ are shown for $T = 0.125$

Appendix C: Scaling of fermion Green's function in the spin glass phase

The pure SYK Green's function admits a conformal solution at low energies, decaying as a power law:

$$G_c(\tau) = \frac{b}{|\mathcal{J}\tau|^{2\Delta}} \,\mathrm{sign}(\tau), \tag{C1}$$

where $\Delta = 1/4$ for the four-fermion SYK model given in Eq. 6. Using a conformal mapping, the finite-temperature solution takes the form

$$G_c(\tau) = b\left[\frac{\pi}{\sin\left(\pi\tau/\beta\right)}\right]^{2\Delta} \mathrm{sign}(\tau). \tag{C2}$$

Numerically, the power-law behavior can be verified by plotting $1/G(\tau)$ as a function of $\sin(\pi\tau/\beta)$ on a log–log scale. For different temperatures T or couplings $\mathcal{J}$, the pure SYK Green's function exhibits a linear region in the log–log plot at large times ($\tau \sim \beta/2$) with an identical slope, reflecting the universal power 2Δ. As T increases, the range over which this linear behavior is observed becomes progressively narrower.

In Fig. 9, we present both the full fermionic Green's function $G(\tau)$ of the coupled problem and the pure SYK Green's function with a static renormalized coupling $\mathcal{J}_{\text{eff}} = V \cdot \langle Q_d^2(\tau)\rangle$. Panels (a) and (b) correspond to $V/J = 1.0$ and $V/J = 5.0$, respectively, for $\Gamma = 2.0$. At very low temperatures, $G(\tau)$ follows the conformal SYK scaling almost exactly at large τ. However, at intermediate temperatures, the slope of $G(\tau)$ at large τ deviates from that of the SYK solution with static $\mathcal{J}_{\text{eff}}$, signaling a departure from pure SYK behavior. As the linear scaling region becomes progressively narrower at higher T, we do not attempt a quantitative extraction of the power law exponent 2Δ.

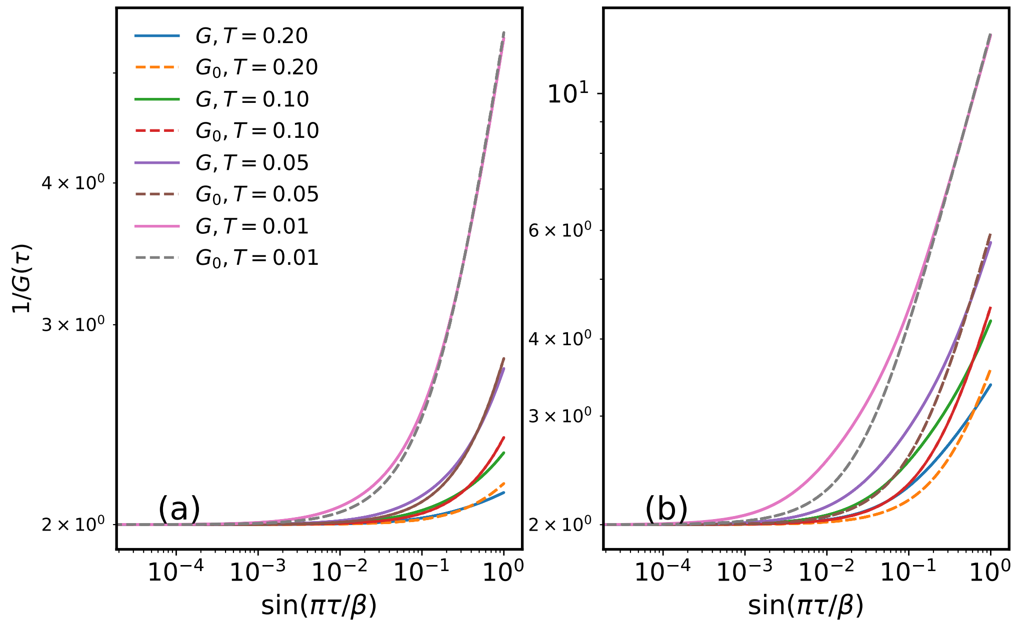

FIG. 9. The fermionic Green's function $G(\tau)$ is shown in Fig. 5(a) and (b), where $1/G(\tau)$ is plotted as a function of $\sin(\pi\tau/\beta)$ on a log–log scale. Panels (a) and (b) correspond to coupling strengths $V/J = 1.0$ and $V/J = 5.0$, respectively, at fixed $\Gamma = 2.0$. For comparison, the Green's function of the pure SYK model with a static effective coupling $\mathcal{J}_{\rm eff}$ is also plotted.

[1] Alexei Kitaev, "A simple model of quantum holography (part 1)," Online talk, Kavli Institute for Theoretical Physics, UC Santa Barbara (2015), part1 of KITP "Entangled" series; available at https://online.kitp.ucsb.edu/online/entangled15/kitaev/.
[2] Alexei Kitaev, "A simple model of quantum holography (part 2)," Online talk, Kavli Institute for Theoretical Physics, UC Santa Barbara (2015), part2 of KITP "Entangled" series; available at https://online.kitp.ucsb.edu/online/entangled15/kitaev2/.
[3] Juan Maldacena and Douglas Stanford, "Remarks on the sachdev-ye-kitaev model," Phys. Rev. D **94**, 106002 (2016).
[4] Debanjan Chowdhury and Brian Swingle, "Onset of many-body chaos in the $o(n)$ model," Physical Review D **96**, 065005 (2017), arXiv:1703.02545 [hep-th].
[5] Yingfei Gu, Andrew Lucas, and Xiao-Liang Qi, "Energy diffusion and the butterfly effect in inhomogeneous syk chains," SciPost Physics **2**, 018 (2017), arXiv:1702.08462 [hep-th].
[6] Jeff Murugan, Douglas Stanford, and Edward Witten, "More on supersymmetric and 2d syk models," Journal of High Energy Physics **2017**, 146 (2017), arXiv:1706.05362 [hep-th].
[7] Pavan Hosur, Xiao-Liang Qi, Daniel A. Roberts, and Beni Yoshida, "Chaos in quantum channels," Journal of High Energy Physics **2016**, 4 (2016).
[8] Debanjan Chowdhury, Antoine Georges, Olivier Parcollet, and Subir Sachdev, "Sachdev-ye-kitaev models and beyond: Window into non-fermi liquids," Rev. Mod. Phys. **94**, 035004 (2022).
[9] Geo Jose, Kangjun Seo, and Bruno Uchoa, "Non-fermi liquid behavior in the sachdev-ye-kitaev model for a one-dimensional incoherent semimetal," Phys. Rev. Res. **4**, 013145 (2022).
[10] Aavishkar A. Patel and Subir Sachdev, "Theory of a planckian metal," Phys. Rev. Lett. **123**, 066601 (2019).
[11] Ehud Altman, Yingfei Gu, Subir Sachdev, and Douglas Stanford, "Sachdev-ye-kitaev models as a platform for strange metal physics," arXiv preprint (2019), arXiv:1908.04795 [cond-mat.str-el].
[12] Tushank Patel, Debanjan Chowdhury, and Subir Sachdev, "Theory of a planckian metal in $2 + 1$ dimensions," Physical Review X **12**, 031048 (2022), arXiv:2203.04990 [cond-mat.str-el].
[13] Xue-Yang Song, Chao-Ming Jian, and Leon Balents, "Strongly correlated metal built from sachdev-ye-kitaev models," Phys. Rev. Lett. **119**, 216601 (2017).
[14] Sean A. Hartnoll and Andrew P. Mackenzie, "Colloquium: Planckian dissipation in metals," Rev. Mod. Phys. **94**, 041002 (2022).
[15] Xie Chen, A. Liam Fitzpatrick, and Eric Kaplan, "Syk-like models with tunable quantum chaos," Journal of High Energy Physics **2017**, 7 (2017), arXiv:1610.08005 [hep-th].
[16] Sumilan Banerjee and Ehud Altman, "Solvable model for a dynamical quantum phase transition from fast to slow scrambling," Phys. Rev. B **95**, 134302 (2017).
[17] Alexei Kitaev and S. Josephine Suh, "The soft mode in the sachdev-ye-kitaev model and its gravity dual," Journal of High Energy Physics **2018**, 183 (2018).
[18] Pak Hang Chris Lau, Chen-Te Ma, Jeff Murugan, and Masaki Tezuka, "On the backreaction of dirac matter in jt gravity and syk model," Physics Letters B **853**, 138702 (2024).
[19] Subir Sachdev and Jinwu Ye, "Gapless spin-fluid ground state in a random quantum heisenberg magnet," Phys. Rev. Lett. **70**, 3339–3342 (1993).
[20] A. Georges, O. Parcollet, and S. Sachdev, "Quantum fluctuations of a nearly critical heisenberg spin glass," Phys. Rev. B **63**, 134406 (2001).
[21] Olivier Parcollet and Antoine Georges, "Non-fermi-liquid regime of a doped mott insulator," Phys. Rev. B **59**, 5341–5360 (1999).
[22] T. R. Kirkpatrick and D. Thirumalai, "Dynamics of the structural glass transition and the p-spin—interaction spin-glass model," Phys. Rev. Lett. **58**, 2091–2094 (1987).
[23] A. Crisanti and H.-J. Sommers, "The sphericalp-spin interaction spin glass model: the statics," Zeitschrift für Physik B Condensed Matter **87**, 341–354 (1992).
[24] Th. M. Nieuwenhuizen, "Quantum description of spherical spins," Phys. Rev. Lett. **74**, 4293–4296 (1995).
[25] Leticia F. Cugliandolo and Gustavo Lozano, "Quantum aging in mean-field models," Phys. Rev. Lett. **80**, 4979–4982 (1998).
[26] Leticia F. Cugliandolo, D. R. Grempel, and Constantino A. da Silva Santos, "Imaginary-time replica formalism study of a quantum spherical p-spin-glass model," Phys. Rev. B **64**, 014403 (2001).
[27] V Dobrosavljevic and D Thirumalai, "1/p expansion for a p-spin interaction spin-glass model in a transverse field," Journal of Physics A: Mathematical and General **23**, L767 (1990).
[28] Subir Sachdev, "Quantum spin glasses and sachdev-ye-kitaev models," (2024), arXiv:2402.17824 [hep-th].
[29] Davide Facoetti, Giulio Biroli, Jorge Kurchan, and David R. Reichman, "Classical glasses, black holes, and strange quantum liquids," Phys. Rev. B **100**, 205108 (2019).
[30] Leticia F. Cugliandolo and Markus Müller, "Quantum glasses," in *Spin Glass Theory and Far Beyond*, Chap. Chapter 18, pp. 353–374.
[31] T. R. Kirkpatrick and P. G. Wolynes, "Stable and metastable states in mean-field potts and structural glasses," Phys. Rev. B **36**, 8552–8564 (1987).
[32] P. G. Wolynes, "Glass dynamics and the energy landscape," J. Res. Natl. Inst. Stand. Technol. **102**, 187–194 (1997).
[33] X. Xia and P. G. Wolynes, "Fragilities of liquids predicted from the random first order transition theory of glasses," Proc. Natl. Acad. Sci. U.S.A. **97**, 2990–2994 (2000).
[34] Yadin Y Goldschmidt, "Solvable model of the quantum spin glass in a transverse field," Physical Review B **41**, 4858 (1990).
[35] Thierry Giamarchi and Pierre Le Doussal, "Variational theory of elastic manifolds with correlated disorder and localization of interacting quantum particles," Physical Review B **53**, 15206 (1996).
[36] Leticia F Cugliandolo and Jorge Kurchan, "Analytical solution of the off-equilibrium dynamics of a long-range spin-glass model," Physical Review Letters **71**, 173

(1993).

[37] Yuxuan Wang, "Solvable strong-coupling quantum-dot model with a non-fermi-liquid pairing transition," Phys. Rev. Lett. **124**, 017002 (2020).

[38] Laura Classen and Andrey Chubukov, "Superconductivity of incoherent electrons in the yukawa sachdev-ye-kitaev model," Phys. Rev. B **104**, 125120 (2021).

[39] Ilya Esterlis and Jörg Schmalian, "Cooper pairing of incoherent electrons: An electron-phonon version of the sachdev-ye-kitaev model," Phys. Rev. B **100**, 115132 (2019).

[40] D. Valentinis, G. A. Inkof, and J. Schmalian, "Bcs to incoherent superconductivity crossover in the yukawa-sachdev-ye-kitaev model on a lattice," Phys. Rev. B **108**, L140501 (2023).

[41] Ilya Esterlis, Haoyu Guo, Aavishkar A. Patel, and Subir Sachdev, "Large-n theory of critical fermi surfaces," Phys. Rev. B **103**, 235129 (2021).

[42] Yuxuan Wang and Andrey V. Chubukov, "Quantum phase transition in the yukawa-syk model," Phys. Rev. Res. **2**, 033084 (2020).

[43] Andrew Davis and Yuxuan Wang, "Quantum chaos and phase transition in the yukawa–sachdev-ye-kitaev model," Phys. Rev. B **107**, 205122 (2023).

[44] Francesco Benini, Tomas Reis, Saman Soltani, and Ziruo Zhang, "$\mathcal{N} = 2$ syk models with dynamical bosons and fermions," (2024), arXiv:2402.08414 [hep-th].

[45] Wenbo Fu, Davide Gaiotto, Juan Maldacena, and Subir Sachdev, "Supersymmetric sachdev-ye-kitaev models," Phys. Rev. D **95**, 026009 (2017).

[46] Anna Biggs, Juan Maldacena, and Vladimir Narovlansky, "A supersymmetric syk model with a curious low energy behavior," Journal of High Energy Physics **2024** (2024), 10.1007/jhep08(2024)124.

[47] Markus Müller and Matthieu Wyart, "Marginal stability in structural, spin, and electron glasses," Annual Review of Condensed Matter Physics **6**, 177–200 (2015).

[48] Surajit Bera, K. Y. Venkata Lokesh, and Sumilan Banerjee, "Quantum-to-classical crossover in many-body chaos and scrambling from relaxation in a glass," Phys. Rev. Lett. **128**, 115302 (2022).

[49] Phil Saad, Stephen H. Shenker, and Douglas Stanford, "A semiclassical ramp in syk and in gravity," (2019), arXiv:1806.06840 [hep-th].

[50] Shao-Kai Jian and Brian Swingle, "Note on entropy dynamics in the brownian syk model," Journal of High Energy Physics **2021**, 42 (2021).

[51] Shenglong Xu and Brian Swingle, "Scrambling dynamics and out-of-time-ordered correlators in quantum many-body systems," PRX Quantum **5**, 010201 (2024).

[52] Leticia F. Cugliandolo and Gustavo Lozano, "Real-time nonequilibrium dynamics of quantum glassy systems," Phys. Rev. B **59**, 915–942 (1999).

[53] L. F. Cugliandolo, D. R. Grempel, G. Lozano, H. Lozza, and C. A. da Silva Santos, "Dissipative effects on quantum glassy systems," Phys. Rev. B **66**, 014444 (2002).

[54] Leticia F Cugliandolo, Gustavo S Lozano, and Nicolás Nessi, "Role of initial conditions in the dynamics of quantum glassy systems," Journal of Statistical Mechanics: Theory and Experiment **2019**, 023301 (2019).

[55] S. J. Thomson, P. Urbani, and M. Schiró, "Quantum quenches in isolated quantum glasses out of equilibrium," Phys. Rev. Lett. **125**, 120602 (2020).

[56] Johannes Lang, Subir Sachdev, and Sebastian Diehl, "Replica symmetry breaking in spin glasses in the replica-free Keldysh formalism," SciPost Phys. **17**, 160 (2024).

[57] Johannes Lang, Subir Sachdev, and Sebastian Diehl, "Numerical renormalization of glassy dynamics," (2025), arXiv:2504.06849 [cond-mat.dis-nn].

[58] Andreas Eberlein, Valentin Kasper, Subir Sachdev, and Julia Steinberg, "Quantum quench of the sachdev-ye-kitaev model," Phys. Rev. B **96**, 205123 (2017).

[59] Ritabrata Bhattacharya, Dileep P. Jatkar, and Nilakash Sorokhaibam, "Quantum quenches and thermalization in syk models," Journal of High Energy Physics **2019**, 66 (2019).

[60] Arijit Haldar, Prosenjit Haldar, Surajit Bera, Ipsita Mandal, and Sumilan Banerjee, "Quench, thermalization, and residual entropy across a non-fermi liquid to fermi liquid transition," Phys. Rev. Res. **2**, 013307 (2020).

[61] Y. Cheipesh, A. I. Pavlov, V. Ohanesjan, K. Schalm, and N. V. Gnezdilov, "Quantum tunneling dynamics in a complex-valued sachdev-ye-kitaev model quench-coupled to a cool bath," Phys. Rev. B **104**, 115134 (2021).

[62] Ancel Larzul and Marco Schiró, "Quenches and (pre)thermalization in a mixed sachdev-ye-kitaev model," Phys. Rev. B **105**, 045105 (2022).

[63] Santiago Salazar Jaramillo, Rishabh Jha, and Stefan Kehrein, "Thermalization of a closed sachdev-ye-kitaev system in the thermodynamic limit," Phys. Rev. B **111**, 195153 (2025).